Journal of Hydrology: Regional Studies 57 (2025) 102183

Contents lists available at ScienceDirect

Journal of Hydrology: Regional Studies

journal homepage: www.elsevier.com/locate/ejrh

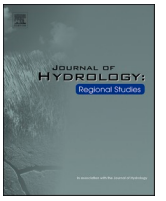

Depositional environment of shallow-marine arenites in the Northern Apennines (Italy) affects aquifer performance: an interpretive key to groundwater management in a climate change scenario

Maria Filippini [a,*], Alessandro Amorosi [a], Enrico Dinelli [a], Stefano Segadelli [b], Laura Landi [a], Tommaso Casati [a], Alessandro Gargini [a]

[a] Biological, Geological and Environmental Science Department, Alma Mater Studiorum University of Bologna, Italy
[b] Geological, Seismic and Soil Survey; Emilia-Romagna region, Bologna, Italy

ARTICLE INFO

Keywords:
Shallow-marine arenitic aquifer
Pantano Formation
Northern Apennines
Aquifer performance
Aquifer yield
Depositional environment
Drought mitigation

ABSTRACT

Study Region: The Pantano Formation arenitic aquifer, in the Northern Apennine chain between Modena and Bologna (Italy).
Study Focus: through an array of geological, hydrogeological and geochemical investigations across distinct members of the Miocene Pantano Formation, this study aims at assessing the influence of depositional environments on aquifer performance (i.e., recharge and storage capacity, spring discharge). As the investigated aquifer represents a key resource for drinking water in the Northern Apennines, interpreting depositional environments might drive future applications in areas understudied from a hydrogeological viewpoint.
New Hydrological Insights for the Region: this study emphasizes the critical role of depositional environments in shaping the aquifer characteristics of the Pantano Formation. Sedimentary facies formed in relatively proximal environments, close to the paleo shoreline, exhibit higher bulk hydraulic conductivity, recharge potential, and storage than those formed in a more distal (open shelf) position, resulting in discharge through larger springs more resilient to droughts. These differences are attributed to depositional factors, such as textural heterogeneity and carbonate content facilitating karst dissolution. Moreover, numerical modeling indicated the feasibility of sustainable groundwater withdrawal though pumping, especially in nearshore sediments, offering a mitigation measure for future water supply challenges during droughts. Therefore, nearshore deposits cropping out in other sectors of the Northern Apennines hold a great potential to mitigate groundwater shortages during droughts and should be the object of further hydrogeological investigations.

1. Introduction

Groundwater is a critical drinking source for nearly two billion people worldwide (Gleeson et al., 2012; WWAP, 2015). The primary underground reservoirs contributing to this vital resource are karst or volcanic aquifers and gravel/sand unconsolidated sediments

* Corresponding author.
E-mail address: maria.filippini3@unibo.it (M. Filippini).

https://doi.org/10.1016/j.ejrh.2025.102183
Received 28 October 2024; Received in revised form 3 January 2025; Accepted 4 January 2025
Available online 10 January 2025

(Goldscheider et al., 2020; Margat and Van der Gun, 2013; Medici et al., 2023; Stevanovicć, 2019). However, other permeable units like hard rock aquifers (Lachassagne et al., 2011; Neuman, 2005; Shakeel et al., 2008) or fractured sedimentary rocks (Bayer et al., 2015; Maliva, 2016; Singhal and Gupta, 2010) can serve as valuable sources of exploitable groundwater under favorable conditions of hydraulic transmissivity, stocked volume and adequate recharge (Cherry et al., 2020; Gargini et al., 2008; Lorenzi et al., 2024; Medici et al., 2024, 2019; van Tonder et al., 2001). Arenites, or sandstones dominated aquifers, are of paramount importance as strategic groundwater reservoirs globally, with 21 out of 37 mega aquifer systems in the planet being associated to sandstone lithology, accounting for around 20–30 % of all fresh groundwater stock of the Earth (Margat and Van der Gun, 2013; Van der Gun, 2022). Among arenitic aquifers, detailed studies have been conducted on alluvial and aeolian sandstones based on pumping tests and sedimentological analyses (Allen et al., 1997; Gossel et al., 2004; Margat and Van der Gun, 2013; Medici et al., 2016, 2019; Powell and Fensham, 2016; Renken, 1996). On the other hand, there are very few references available about shallow-marine sandstone aquifers (Runkel et al., 2006).

Climate change can significantly impact groundwater flow systems in mountainous regions, especially in highly heterogeneous and anisotropic sedimentary aquifers (Green et al., 2011; Stigter et al., 2023). Areas reliant on these aquifers as the only high-quality reservoirs are facing increasingly critical issues, as cyclic droughts induced by climate change disrupt the space-time dynamics of recharge, leading to severe shortages in spring discharge and public water supply (Amanambu et al., 2020; Atawneh et al., 2021; Caloiero et al., 2018; Dore, 2005; Kundzewicz and Doli, 2009; Riedel and Weber, 2020; Tambe et al., 2012; Weissinger et al., 2016). To manage groundwater use effectively and implement sustainable development measures, it becomes essential to identify aquifer units resilient to climate effects (Cuthbert et al., 2019; Scanlon et al., 2023; Taylor et al., 2013).

The Northern Apennine mountain chain provides a representative case study for these critical issues. In this region, sedimentary rocks dominate, accounting for 96 % of the total outcrop area of aquifers, which is equal to 14,600 km^2 (Gargini et al., 2014). The Northern Apennine region, located near the southern edge of the European continent in the Mediterranean basin, has experienced increasingly frequent and intense droughts with a cycle of five years since the start of the XXI century (Filippini et al., 2024; Peña-Angulo et al., 2022; Rakovec et al., 2022; Riedel and Weber, 2020). The adverse effects include reduced spring discharge,

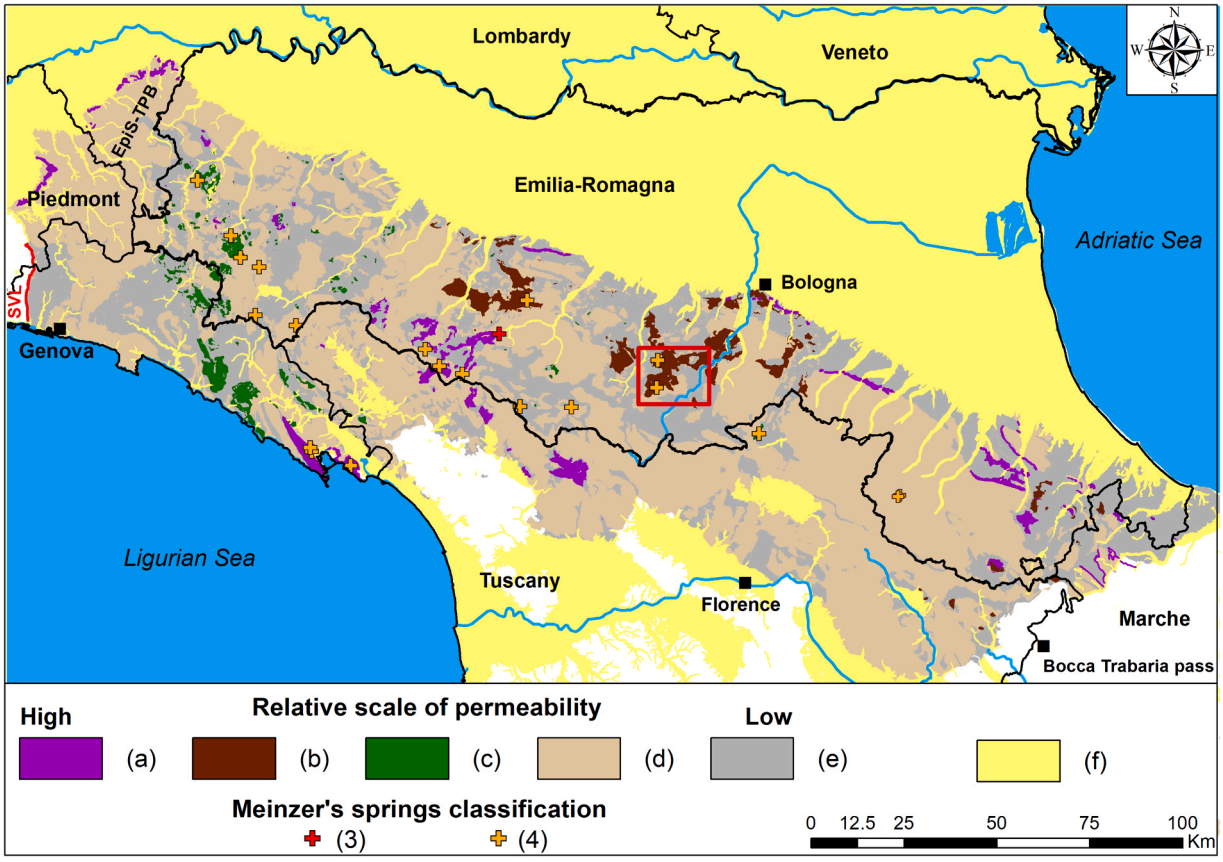

Fig. 1. Hydrogeological categories along the Northern Apennines: a) karst aquifers made of evaporites and limestones; b) arenitic fractured aquifers (Pantano Formation – focus of this study); c) igneous and metamorphic fractured aquifers; d) turbidite fractured aquifers (arenaceous, arenaceous-pelitic, or calcareous-marly), and molassic deposits; e) rock units with behavior of aquitard or aquiclude; f) unconsolidated deposits (alluvial plains, river valleys, inter-mountainous basins). The springs pertaining to Meinzer's Class III and IV are shown on the map. The study area of this paper is framed in red.

conflicts between various ecosystem services provided by groundwater leading to impaired environmental flows in rivers, and the need to use water tankers to supply villages in the countryside. It is noteworthy that adverse effects of droughts seem to impact differently within aquifer settings of similar lithology (e.g. arenitic aquifers). A key to interpret this variability is needed in order to better address mitigation measures.

This research focuses on the comparative analysis of sedimentological, geochemical and hydrogeological indicators along a depositional transect of a shallow-marine (shoreface to shelf) arenite between the provinces of Bologna and Modena (Northern Apennines, Emilia Romagna Region, Italy), with a twofold goal:

(I) Through hydrological and geochemical analysis of spring discharge, borehole logging and hydraulic tests, the study aims to investigate the depositional environment of sandy deposits relative in terms of distance from the paleo shoreline, as a key factor that may influence the performance of the arenitic aquifer. "Aquifer performance" is defined by Pierce et al. (2013) as a combination of three factors: (1) recharge rate and storage conditions, (2) water quality, (3) discharge rates and environmental flow. As water quality is not an issue in the investigated setting, considerations were carried out based on recharge-storage and discharge conditions;

(II) Through Numerical modeling of groundwater flow in critical sectors of the investigated aquifer, the work aims to provide a tool for knowledge transfer from science to groundwater management applications, by suggesting scenarios of sustainable pumping to integrate the groundwater demand for human needs in a region prone to the effects of recurrent droughts induced by climate change.

2. Geological and hydrogeological setting

2.1. The Northern Apennines

The Northern Apennines consist of a variety of lithostratigraphic units that accumulated into a series of paleogeographic domains along NW-SE striking and NE-verging thrusts (Boccaletti et al., 1985; Ricci Lucchi, 1986). From a hydrogeological perspective, the complex pattern of geological units that form the Northern Apennines was classified into six categories, from "a" to "f", based on (i) the relative proportion of dissolution processes, (ii) the sandstone-calcarenite to mudstone-marl ratio for sedimentary rocks, and (iii) the relative abundance of major springs per unit area (Fig. 1). Groups "a" to "d" represent aquifer units with decreasing relative permeability, whereas group "e" represents aquitards or aquicludes (mud-bearing to mud-dominated lithostratigraphic units made of marls, mudstones and clayey complexes). Group "f" refers to unconsolidated deposits (alluvial plains, river valleys, and inter-mountainous basins) that were not considered for hydrogeological classification. In detail, group "a" includes karst aquifers made of gypsum (e.g., Chiesi et al., 2010) and carbonate rocks characterized by widespread dissolution processes (Triassic and Messinian formations), and limestone successions potentially subject to corrosion (Late Jurassic to Middle Eocene formations). Group "b", the main focus of this paper, consists almost entirely of fractured sedimentary (arenitic) aquifers pertaining to the Pantano Formation (Upper Burdigalian to Lower Langhian; details in Section 2.2). The calcite-rich composition of the Pantano arenite, along with its homogeneous lithology, make it prone to dissolution with local enlargement of fractures (Filippini et al., 2024). Group "c" includes igneous and metamorphic rock aquifers, such as peridotite, serpentinized peridotite, gabbro, and basalt, which occur as scattered outcrops (olistolites) embedded within low-permeability units. Although these rocks are not prone to corrosion, they are highly fractured and exhibit significant primary porosity, resulting in an overall significant permeability (Segadelli et al., 2021, 2017a, 2017b). Group "d" is the dominant type of aquifer in the Northern Apennine chain and the one with the lowest relative permeability (Gargini et al., 2008). It mostly consists of fractured turbidites with arenaceous, arenaceous-pelitic, or calcareous-marly composition (Early Cretaceous to Oligo-Miocene formations) and, to a minor extent, of Middle Pliocene-Early Pleistocene molassic deposits.

Out of the total rocky aquifer outcrops in the Northern Apennines, only 7.5 % pertains to the three high-permeability groups (a, b, c). This highlights the overall low aquifer performance throughout the region. The distribution of major springs discharging from rock units, excluding those arising from debris or glacial deposits, further supports this observation (Fig. 1). According to Meinzer's classification (Meinzer, 1923), which ranks springs based on discharge rates during the low-flow season, Class I or II springs (corresponding to low-flow discharge $> 10{,}000$ L/s and > 1000 L/s, respectively) are not represented in the area. The only one Class III spring (low-flow discharge > 100 L/s) originates from group "a". Twelve out of 20 springs pertaining to Class IV (low-flow discharge $>$ 10 L/s) arise from the three most permeable aquifer groups "a", "b" and "c", while only 8 are associated with the extensively represented group "d". Notably, three of the Class IV springs discharge from group "b", focus of this study, despite its limited extent.

2.2. Depositional setting of Pantano Formation

The Pantano Formation, about 350 m thick, forms the lower part (Upper Burdigalian-Lower Langhian) of the Miocene Bismantova Group, which also includes the Upper Langhian to Upper Serravallian Cigarello Formation. A regional unconformity, marking the erosional truncation of older Epiligurian units, constitutes the base of the Pantano Formation. The Bismantova Group has a varied facies architecture: it accumulated within a series of wedge-top basins (Ricci Lucchi, 1986) and, as a whole, records a characteristic deepening upward-tendency, from coastal and inner-shelf deposits (Pantano Formation) to outer-shelf and slope marls (Cigarello Formation). The shelf deposits of the Pantano Formation represent a stratigraphic marker that can be traced across the entire Northern Apennines through a dominantly turbidite foreland-basin succession (Amorosi, 1997). The generalized drowning of shelves during the Late Langhian-Early Serravallian was accompanied by the rapid transition from hybrid (carbonate+siliciclastic) arenites to predominantly siliciclastic deposits and by the development of a characteristic condensed horizon rich in glaucony, at the boundary between Pantano and Cigarello formations (Amorosi, 1995).

The area investigated in this paper consists of an extensive outcrop of the Bismantova Group, covering approximately 70 km^2

(Fig. 2). In this area, the Pantano Formation unconformably overlies the Epiligurian Contignaco Formation and is overlain, in turn, by the Cigarello Formation. In the westernmost sector of the study area, the Pantano Formation consists of a typical bioclastic arenite that can be subdivided into two lower-rank lithostratigraphic units: the Sassoguidano Member (PAT1) and the overlying Montecuccolo Member (PAT2). PAT1 is a fine- to medium-grained calcarenite that exhibits a progradational stacking pattern with an overall shallowing-upward trend. It displays a typical cyclic facies architecture, with burrowed and structureless very fine arenites in vertical transition to coarser-grained, more proximal, wavy-bedded, inner-shelf to shoreface/foreshore deposits. The stratigraphic unconformity that separates PAT1 from PAT2 is the base of transgressive, glaucony-rich, tide-dominated and storm-influenced nearshore arenites, with a characteristic coarser grain size, locally marked by a transgressive pebble layer (Amorosi, 1997). In the easternmost sector of the area, the Pantano Formation has different lithologic and sedimentological characteristics (PAT in Fig. 2) that have interpreted to reflect the transition from marginal-marine and inner-shelf arenites (PAT 1, PAT2) to highly bioturbated sandstones and siltstones formed in relatively deeper water settings. Sedimentary structures in PAT have mostly been obliterated by intense bioturbation and the lithofacies assemblage is highly homogeneous. Overall, PAT represents the distal equivalent of PAT1 and PAT2, from which it can be distinguished by its lower grain size and carbonate content.

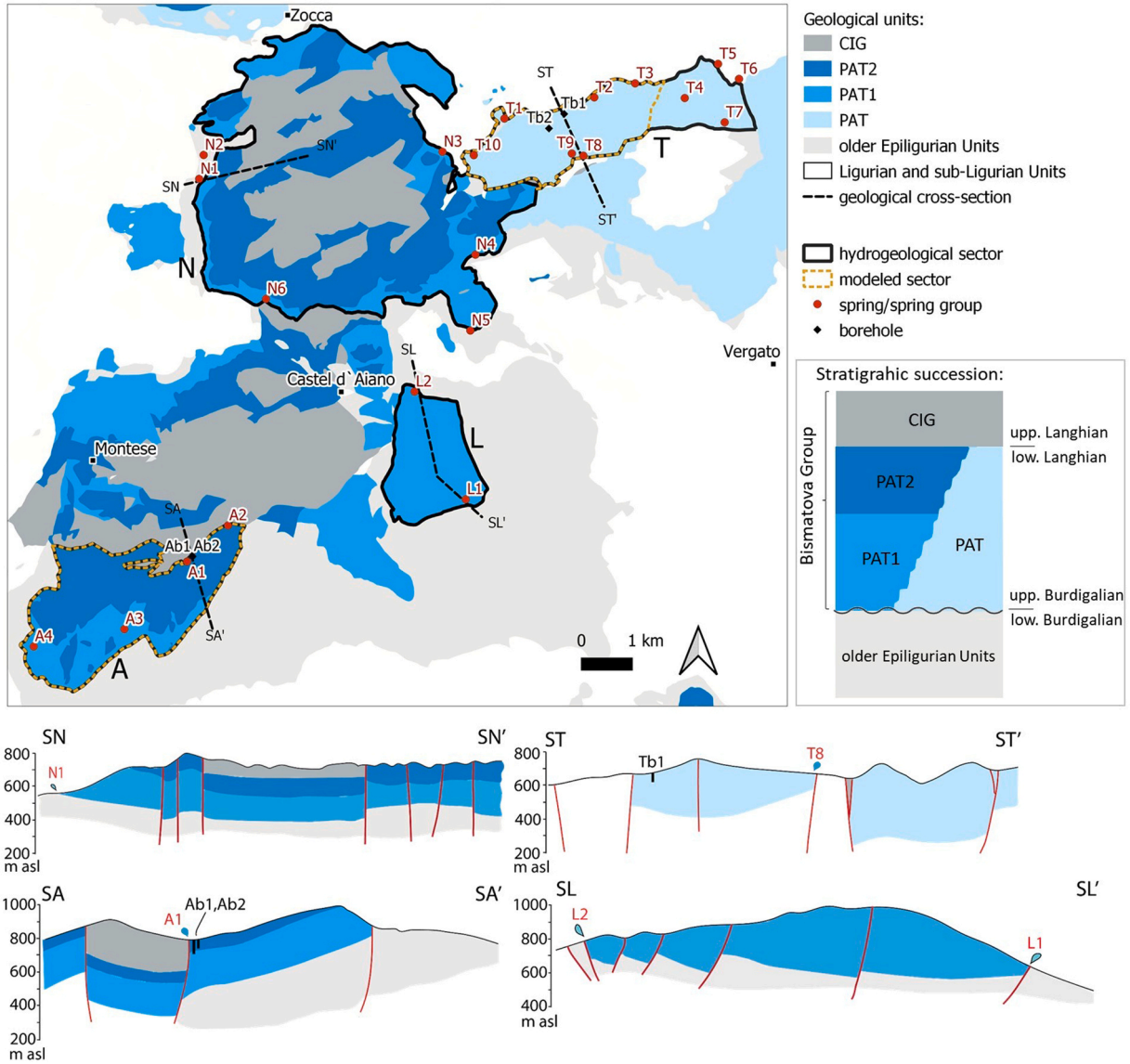

Fig. 2. Geology of the study area. The monitored springs and boreholes are indicated on the map. The hydrogeological sectors of interest for the study are highlighted together with the sectors considered for numerical flow modeling. A simplified geological cross-section is represented for each hydrogeological sector. The local stratigraphic succession is sketched on the right (modified from Panini et al., 2003).

3. Methods

3.1. Coring, rock sampling, and borehole inspection

Two boreholes were drilled between November and December 2021 nearby one of the main spring discharge points in the westernmost sector of the investigated area (A1 in Fig. 2). The two boreholes, namely Ab1 and Ab2, are spaced apart of 10 m. Ab1 was drilled down to 80 m bgs using a wireline continuous coring system with single tube core barrel of 101 mm diameter that provided consistent, high core recovery of 90–100 % in the hard rock intervals. Ab1 required permanent casing down to 49 m during drilling to ensure stability of the borehole due to the presence of an inconsistent layer between 31 and 49 m bgs. Borehole Ab2 was bored using a core destruction probe with a diameter of 101 mm down to a depth of 35 m bgs.

A total of 20 rock samples were recovered from core Ab1 and additional 27 rock samples were collected in outcrops close to the springs (details in the Supplementary Material, "SM" hereafter) in order to evaluate bulk rock geochemical composition. Samples were crushed, milled and prepared as powder pellets for the chemical analysis performed using a Panalytical Axios 4000 wavelength dispersive X-ray fluorescence (XRF) spectrometer equipped with a Rh tube at the XRF laboratory of BiGeA Department, Bologna. The reproducibility of the major elements was generally better than 5 %, while it was better than 10 % on average for trace elements. The Loss On Ignition (LOI) was gravimetrically estimated after 12 h heating at 950 °C in a muffle furnace (Heiri et al., 2001).

Vertical logging with mechanical caliper, optical and acoustic televiewer was performed along the uncased boreholes to observe the distribution, setting and aperture of the main geological discontinuities, plausibly contributing to groundwater flow (Maurice et al., 2012). The logging was performed by a private company (Waterstones S.r.l.)

The two boreholes were completed with a 4" ID PVC piezometric tube screened from 49 to 80 m bgs in Ab1 and from 2 to 30 m bgs in Ab2. The annular space around the screened tubes was backfilled with siliciclastic gravel with size range 2–5 mm. In Ab1, the annular space along the cased sector (0–49 m bgs) was sealed with a mixture of bentonite and concrete.

3.2. Hydraulic tests in boreholes

3.2.1. Pumping and recovery tests

Pumping and recovery tests were performed in Ab1 and Ab2 (see Section 3.1) and in two existing wells, namely Tb1 and Tb2, located in the easternmost sector of the area (Fig. 2). The two wells are 40 m deep and are used to provide drinking water through public fountains. The tests were performed between April 20th and July 12th 2022 with a variable duration of 5–46 h, including the pumping and recovery phases. Technical details of each test are reported in the SM. In summary, pumping was applied at a constant rate of 0.7–1.1 L/s depending on the test site. In the case of Ab1 and Ab2, a submersible pump was inserted in the piezometers for the duration of the pumping test, while in Tb1 and Tb2 the pumping was performed using the submersible pump already in use in the wells. These were turned off at least 24 h in advance to ensure an unperturbed condition at the beginning of the test. Hydraulic head was monitored using pressure transducers (Onset HOBO, models U20L-09, 20L-04) with a 30 s acquisition interval. The hydraulic head in the well or piezometer adjacent to the pumping point was also monitored for observation.

In the case of the Tb1 test, the aquifer hydraulic transmissivity was derived by fitting either the pumping and recovery experimental data with the non-equilibrium log approximation of the Theis model for confined aquifers (Kruseman and Ridder, 1990). The transmissivities derived from pumping and recovery (T_P and T_R, respectively) were averaged to obtain a transmissivity (T) representative of the test site. In the Tb2 test, only the recovery phase was analyzed due to strong head losses occurred in the well during pumping. For Ab1 and Ab2 tests, T_P was estimated by fitting the experimental data to the equilibrium Thiem model (Tügel et al., 2016) due to early stabilization of the drawdown, while T_R was derived using the aforementioned approximation of the Theis model. Hydraulic conductivity (K) was derived by dividing T over the screen length of the tested well/piezometer. When drawdown was registered in the observation point adjacent to the pumping station, a Storativity (s) was also estimated using the Theis log approximation model.

3.2.2. Vertical hydraulic logging

Vertical hydraulic logging (VHL) was carried out in Ab1 and Ab2 by a private company (Waterstones S.r.l.) utilizing a micro-impeller spinner flow meter along the uncased sectors of the boreholes before their completion with piezometric tubes. The spinner flow meter measures the downhole vertical component of groundwater flow's apparent velocity, based on the rotational speed of a vertically oriented helical axis (Molz et al., 1994). Such analysis aids in identifying the vertical distribution of active groundwater flow along a borehole. The hydraulic logging took place under either ambient or dynamic conditions. In the dynamic scenario, a pumping rate of 1.76 L/s and 1.36 L/s was respectively applied to Ab1 and Ab2 using a submersible pump positioned at a depth of 10 and 7 m bgs.

3.3. Spring discharge monitoring

Discharge monitoring was conducted across a network of 22 springs or groups of springs from September 2020 to January 2022 (Fig. 2, and further detail in the SM). By "group of springs", we refer to spatially clustered point-type outlets sharing similar hydrogeological and hydrochemical characteristics. The selection involved an initial assessment of the existing spring database managed by regulatory agencies, followed by on-site field assessments to determine the current conditions of springs. The majority of the selected springs are perennial and are either partially or entirely exploited by the main water company or by smaller private aqueducts. Each

spring was tentatively associated with the prevalent lithology of its contributing area, forming three groups: PAT, PAT1, PAT1 +PAT2. For each monitoring point, a variable number of discharge measurements were taken between 23 and 2 (average of 12). Discharge was measured either with the volumetric method (i.e., measuring the time needed to fill a graduated container) or the velocity-area method (Herschy, 1993), depending on the spring flow magnitude and logistic constraints. In the latter method, flow velocities were measured utilizing an Acoustic Doppler Velocimeter (*Flowtracker, SonTek/YSI Inc*). All discharge measurements account for the total spring outflow, inclusive of the aqueduct uptake and potential overflow.

Three indicators were defined for each spring considering the discharge monitoring of the hydrological year 2020–21 (the only year covered entirely by the monitoring, i.e. from November 2020 to October 2021). The indicators are: (1) mean discharge during the recession limb of the spring hydrograph (Recession Mean Discharge or RMD, hereafter), that was used to classify the springs following Meinzer (1923); (2) coefficient of recession α, according to the Maillet's exponential model (Maillet, 1905; Medici et al., 2023) which has previously been shown to accurately represent the recession response of most Northern Apennine springs (Filippini et al., 2024; Gargini et al., 2008; Segadelli et al., 2021); and (3) index of discharge variability (I_v), corresponding to the ratio Q_{max}/Q_{min} (Kresic and Stevanovic, 2010). The first two indicators refer to the discharge recession phase from August to October 2021 (i.e., the final stage of the depletion limb of the hydrograph where discharge is solely contributed by groundwater from the aquifer with no perturbation induced by active direct recharge or fast-flow from the surface). This phase is considered the most critical, as this is when the water supply from the springs typically faces periodic shortages. The third indicator is representative of the entire hydrological year.

To note that six of the 22 springs were added to the monitoring program later, during the summer of 2021, due to logistical constraints, such as unfavorable field conditions or restricted access by private owners. These springs have a relatively low number of discharge measurements, ranging from 2 to 9 (see SM for details). I_v was not calculated for these six cases, as the data were not evenly distributed across the hydrologic year (i.e., at least one measurement per season was required). On the other hand, α was calculated when at least four discharge measurements were taken between August and October 2021.

3.4. Hydrologic budget

Distinct aquifer sectors were identified in the investigated area plausibly independent in terms of hydrologic budget based on the occurrence of permeability limits such as the contact with aquitard lithologies. For the hydrologic year 2020–21 (i.e. from November 2020 to October 2021), the primary inflows and outflows of groundwater were estimated within each sector. The principal inflow was determined as effective precipitation (P_e), which accounts for total precipitation adjusted for actual evapotranspiration. Lateral recharge from rivers was assumed negligible since significant watercourses do not intersect these sectors. The actual evapotranspiration was calculated using the Thornthwaite & Mather approach (Steenhuis and Van Der Molen, 1986; Thornthwaite and Mather, 1957) assuming a 100 mm of available water in the soil zone. Correlations were established between P_e and the altitude above sea level. The correlations were derived using data from various meteorological stations at different altitudes along the Apennine range between the Panaro and Reno Rivers, and were exploited to spatialize P_e over the investigated sectors based on altitude (see SM for more details). Mean spring discharge recorded during the 2020–21 year was considered as the primary outflow. We excluded the occurrence of substantial lateral flow towards other aquifer sectors due to unfavorable geological configurations. The total discharge (TD) of each sector was calculated as the sum of the mean annual discharges of the monitored springs within that sector, with an increment of 20 % to account for non-surveyed discharge points. Knowing the outcropping area of the aquifer units in each sector, and assuming steady state conditions at the scale of a hydrologic year (as previously observed for the Northern Apennine springs; Cervi et al., 2018; Gargini et al., 2008; Segadelli et al., 2021), it was possible to estimate the coefficient of effective infiltration (C_{EI}) as the ratio between yearly inflow (i.e., recharge) and outflow (i.e., discharge).

3.5. Groundwater sampling and analysis

Groundwater samples were collected for the analysis of major ions (Ca, Mg, Na, K, Cl, SO_4, HCO_3) from the 22 springs or groups of springs already selected for discharge monitoring (see Section 3.3). Sixteen out of the 22 springs were sampled twice: in May 2021 and in October 2021. The remaining 6 springs, corresponding to those added to the discharge monitoring program during the summer of 2021 (see Section 3.3 and SM), were sampled only during the October campaign. Spring water was collected at the groundwater outlet using two 250 mL PET bottles. Of the two samples, one was left non-acidified (for anion analysis), while the second one was acidified to pH 2 using HCl (for cation analysis). Samples were kept cool (4–10°C) until analysis. The water samples were analyzed at the Laboratory of the GruppoHERA water company following the standard methods EPA 300.1 1997 and APAT-CNR-IRSA 29/2003 (sections 2010, 2090, 3010, 3020). Trace elements were analyzed from an additional field-filtered, acidified sample (250 mL PET bottle) collected from the 22 springs during the October campaign. The analyses were performed using a Perkin-Elmer DRCe ICP-MS spectrometer at the 'Bruno Capaccioni' Geochemistry Lab of the BiGeA Department. (details on trace elements are in the SM). Four out of the 22 springs or spring groups were additionally sampled in March 2023 for tritium (^3H) analysis within the water molecule. The selected springs are the most productive within the study area. Samples were collected in 1 L PE bottles, stored at 4°C and delivered to the lab the day after collection. The analysis was conducted at the Chemistry-Isotopic Lab of the Institute of Geosciences and Earth Resources of the National Research Council of Italy (CNR-IGG, Pisa) using a Perkin Elmer Quantulus liquid scintillation counter based on the electrolytic enrichment method (Schäfer et al., 2000). The results are reported as tritium units (TU; where 1 TU equals 1 molecule of ^3H_1HO per 1018 molecules of ^1H_2O) with an analytical precision ranging from 0.4 to 0.5 TU.

Water temperature (T), electrical conductivity compensated at 20°C (EC), and pH were measured at each sampling point using a multiparametric probe (HI991301-Hanna Inc) in conjunction with every spring discharge measurement (see Section 3.3). Total

Dissolved Solids (TDS) values were estimated from EC using a conversion factor of 0.64 (e.g., Atekwana et al., 2004; Hubert and Wolkersdorfer, 2015), and normalized to Cl to assess the potential for water-rock interaction. A higher normalized value suggests a greater potential for water-rock interaction, assuming the origin of Cl is not related to mineral dissolution (Miller, 1999, 2002).

3.6. Groundwater flow modeling

On the westernmost and easternmost sectors of the investigated area (A and T in Fig. 2), two finite-difference groundwater flow numerical models were implemented using MODFLOW-2005 (Harbaugh, 2005) to explore the potential for integrating the spring-based public water supply during droughts through the use of pumping wells.

The two modeled sectors were discretized using a grid of 5 × 5 m cells on the horizontal plane. The total thickness of the models extends from the ground surface to the base of Pantano Formation (i.e. the aquifer) and was divided in 2–3 layers representing different members of the formation (Fig. 2), whose surfaces were interpolated on nets of geological sections in the SW-NE and NW-SE direction.

An equivalent porous medium (EPM) approach was used to model the fractured aquifers by assigning bulk hydrogeological properties (K, S_y), that were increased in correspondence of main fault zones. Such approach is widely employed to model groundwater flow in fractured aquifers at a scale of 1–10 km (e.g., Abusaada and Sauter, 2013; Folch and Mas-Pla, 2008; Medici et al., 2021; Michael and Voss, 2009; Nastev et al., 2005). The bulk K for the two models is within 4.5 × 10–7 m/s and 4.5 × 10–6 m/s, while fault zones are characterized by higher K in the range of 1.5 × 10–5 m/s and 1.5 × 10–4 m/s. The bulk Sy for the two models is within 0.11 % and 2 %.

Groundwater flow was simulated in a transient state, using 12 monthly stress periods. Transitory groundwater recharge was defined through the estimation of mean monthly recharge values between November 2020 and October 2021. Springs were simulated as constant head cells and the discharge measurements conducted during the hydrologic year 2020–21 (see Section 3.3) were used to constrain the models (as in, e.g., Manga, 1997; Martínez-Santos et al., 2014; Saar and Manga, 2004) through a trial-and-errors calibration process (Abdelhalim et al., 2019; Scanlon et al., 2003; Sophocleous et al., 1999; Zhou et al., 2014). The calibration performance

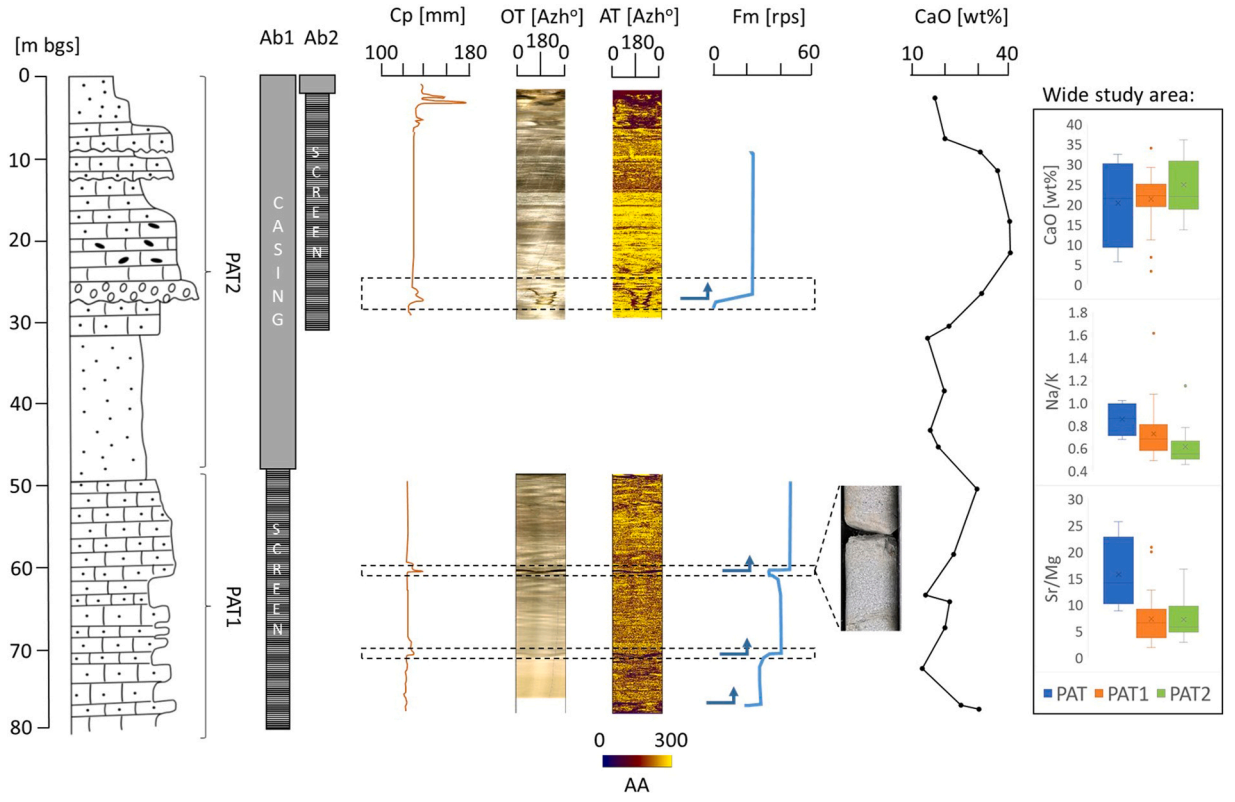

Fig. 3. Vertical logging of the Ab1 and Ab2 boreholes. From the right: geological logging (Ab1); completion of boreholes with casing and screens; Caliper logging ("Cp"); Optical Televiewer logging ("OT"); Acoustic Televiewer logging ("AT"); dynamic Flowmeter logging ("Fm"); core picture showing the irregular surfaces of an open fracture at 61 m bgs; calcium oxide profile from rocks sampled along Ab1 (CaO). Cp, OT, AT, and Fm were performed along Ab2 (2–30 m bgs) and Ab1 (49–80 m bgs). OT and AT show the entire borehole wall from Azimuth (Azth) 0° to 0° in a clockwise direction. The color scale of AT represents the Acoustic signal Amplitude (AA). Black dashed lines frame the intervals of active groundwater flow as deduced by vertical logging, i.e. open fractures and water inflows registered during the dynamic Fm (highlighted with blue arrows). On the right hand side, boxplots show CaO, Na/K, and Sr/Mg from all rock samples (including samples collected from outcrops in around the study area). Na/K and Sr/Mg ratios were determined on molar concentrations, with Sr concentrations multiplied by 1000.

was quantified by calculating the NRMSE, i.e., the ratio between the root mean squared error and the range of observed values. A NRMSE < 10 % is typically considered indicative of good calibration (Anderson et al., 2015).

The numerical setup of the year 2020–21 was replicated five times, resulting in a total of 60 stress periods, to extend the model duration to five years. This duration was chosen to capture the typical periodicity of droughts in the region, which occur approximately every five years, likely due to climatic cyclicality associated with ENSO (El Niño-Southern Oscillation; Trenberth et al., 2007).

Two pumping wells were provisionally incorporated into each of the two five-year models. In the A sector, the wells were positioned along a principal fault zone at a depth of 120 m, each operating with a pumping rate of 2.5 L/s. Similarly, in the T sector two wells were situated in a region of converging flow along the northeastern border of the aquifer, at a depth of 150 m, each with a pumping rate of 1.0 L/s. To depict the worst-case scenario of a prolonged drought without interruption between two successive ENSO cycles, the wells were operational throughout the entire five-year modeling period, for five months each year (June to October), corresponding to the critical period wherein there is a potential need for water supply supplementation via pumping.

Transitory recharge estimated for the hydrologic year between November 2021 and October 2022 was later used to predict groundwater flow in a critical climatic scenario. Indeed, year 2021–22 was identified as climatic stress test because of its particularly severe drought conditions. The same pumping scenario described above was applied on this new model setup. Further details on model implementation are in the SM.

4. Results

4.1. Sediment core, bulk rock geochemistry, and borehole observations

Core Ab1 (Fig. 3) penetrated approximately 80 m of the Pantano Formation. As stratification shows a NNE dipping with a dip angle of 30° in the coring area, this likely represents an apparent rather than true thickness. Only facies PAT1 (30 m) and PAT2 (50 m) were encountered, in the lower and upper parts of the core, respectively. Based on facies analysis of core Ab1 and nearby scattered outcrops, PAT1 in the study area is a fine-grained, grey calcarenite, characterized by distinctive coarsening-upward cycles, with wave ripples and hummocky-cross stratification; whereas PAT2 is coarser-grained, more altered and brownish in color, rich in pebbles, bioclasts and glaucony, and shows and abundance of trough and planar cross-stratification, with distinctive fining-upward trends. The rock geochemical composition of the Pantano Formation is dominated by CaO, as testified by data of core Ab1 and from the entire sample population, showing similar ranges among members and an average of 22.4 wt% (Fig. 3). The three members can be differentiated on the basis of their Na/K and Sr/Mg ratios, both decreasing from PAT to PAT1 to PAT2. These ratios were selected as they allow a comparison with water chemistry (see Section 4.5.1).

In borehole Ab2, intercepting PAT2, the caliper and televiewer logs show that the shallowest section (0–7 m bgs) is characterized by an irregular diameter and a numerous fractures, likely representing the altered surface zone of the rock mass (Fig. 3). Below this depth (7–30 m bgs), relatively few fractures were observed, with the main ones visible in both the optical and acoustic televiewers between 26 and 29 m bgs and associated with slight variations in borehole diameter. In Ab1 (49–80 m bgs) fewer fractures are observed compared to Ab2. The caliper detects two main enlargements at depths of 61 and 71 m bgs, respectively. At the same depths, the televiewers observed fractures with significant apertures, ranging from 15 to 20 cm. The fracture surfaces observed on the core at these depths are irregular, suggesting chemical dissolution of the carbonate matrix of the arenite (Fig. 3). All the major fractures along Ab1 and Ab2 have Apennine (NW-SE) or anti-Apennine (SW-NE) orientations, consistent with previous outcrop observations in the study area (Balocchi, 2014; Filippini et al., 2024).

4.2. Hydraulic tests in boreholes

The Ab1 and Ab2 pumping and recovery tests allowed estimating a T value of 3e-3 m2/s in the westernmost sector of the study area, corresponding to a bulk K of 1e-4 m/s (Table 1). Similar results obtained from these two tests suggest that there is no appreciable difference between PAT1 (screened by Ab1) and PAT2 (screened by Ab2) in terms of aquifer transmissivity. During both pumping tests, a drawdown was registered in the adjacent observation piezometer allowing an estimation of S between 5e-5 (Ab1 test) and 3e-2 (Ab2 test). The difference in S is most likely attributable to the depth of the screen in the pumping piezometer. Ab1, which has a deeper screen, suggests an S value characteristic of a confined aquifer (i.e., Specific Storage, related to fluid and rock compressibility). In contrast, Ab2 shows an S value more typical of an unconfined aquifer (i.e., Specific Yield, associated with water drainage under the force of gravity). The estimated T in the easternmost sector is generally lower than to the west, with a value of 6e-4 m2/s for the Tb1

Table 1
Hydrogeological properties derived from pumping and recovery tests in boreholes Tb1, Tb2, Ab1, Ab2. T_P and T_R are hydraulic tansmissivities estimated from the pumping and recovery phase, respectively. T is the average between T_P and T_R. K_{buk} is the bulk hydraulic conductivity derived by dividing T for the length of the well screen. S is the storativity. ND indicates not determined parameters.

	T_P [m^2/s]	T_R [m^2/s]	T [m^2/s]	K_{bulk} [m/s]	S
Tb1	$5E^{-4}$	$7E^{-4}$	$6E^{-4}$	$3E^{-5}$	ND
Tb2	ND	$6E^{-5}$	$6E^{-5}$	$2E^{-6}$	ND
Ab1	$2E^{-3}$	$4E^{-3}$	$3E^{-3}$	$1E^{-4}$	$5E^{-5}$
Ab2	$2E^{-3}$	$4E^{-3}$	$3E^{-3}$	$1E^{-4}$	$3E^{-2}$

test (corresponding to a bulk K of 3e-5 m/s), and 6e-5 m2/s for Tb2 (bulk K of 2e-6 m/s). Since both wells are screened in the same lithology (PAT), the difference in T must be due to varying structural conditions. Specifically, Tb1 is located in the damage zone of a major extensional fault (Panini et al., 2003), which likely increases the permeability of the rock mass, whereas Tb2 is situated in undamaged rock mass. In the two Tb tests, drawdown was not detected in the observation well, probably due to the lower aquifer transmissivity and to the greater distance between the pumping and observation wells (415 m) compared to the western region (10 m). Consequently, it was not possible to estimate S.

The vertical hydraulic logging conducted under ambient conditions did not reveal evidence of flow in Ab1 nor in Ab2, suggesting the absence of significant vertical flow components along the boreholes. In contrast, dynamic logging identified few narrow sections in the tested boreholes with concentrated vertical inflows (Fig. 3). In Ab1, groundwater inflow occurs around 80 m bgs (i.e. the borehole bottom), contributing to 55 % of the total inflow induced by pumping, and between 61 and 71 m bgs, contributing to the remaining 45 %. In Ab2, nearly all inflow occurs between 27.5 and 28.5 m bgs. These depths correspond to zones with open fractures or fracture sets, as previously identified by caliper and televiewer logging (see Section 4.1).

4.3. Spring discharge analysis

The measured spring discharge values range from 0.1 to 66.7 L/s. The number of measurements for each spring and other details about the monitoring campaign are in the SM. Springs with higher RMD are predominantly fed by PAT1+PAT2 (RMD between 2 and 46 L/s, with an average of 13 L/s), followed by PAT1 (0.5–7 L/s, with an average of 3 L/s). Springs fed by PAT show the generally lowest values (0.1–4 L/s, with an average of 1 L/s) (Fig. 4). Most of the springs (20 out of 22) fall within class V of Meinzer (1923), corresponding to RMD between 1 and 10 L/s, while the remaining two (N1 and A1) fall within class IV, with RMD between 10 and 100 L/s. The coefficient α was calculated for 20 out of 22 springs that had at least 4 measurements during the recession season. The range of variation among the 20 springs spans approximately one order of magnitude, from 2e-2–1e-3 d^{-1}. Low values are generally associated with the PAT1+PAT2 and PAT1 lithologies (averages of 4e-3 and 5e-3 d^{-1}, respectively) whereas higher values are found in the PAT springs (with an average of 8e-3 d^{-1}). I_v was calculated for 16 out of 22 springs, where at least one measurement was available for each season of the hydrological year (i.e., Nov-Jan, Feb-Apr, May-Jul, Aug-Oct) to obtain a reliable estimate of the annual

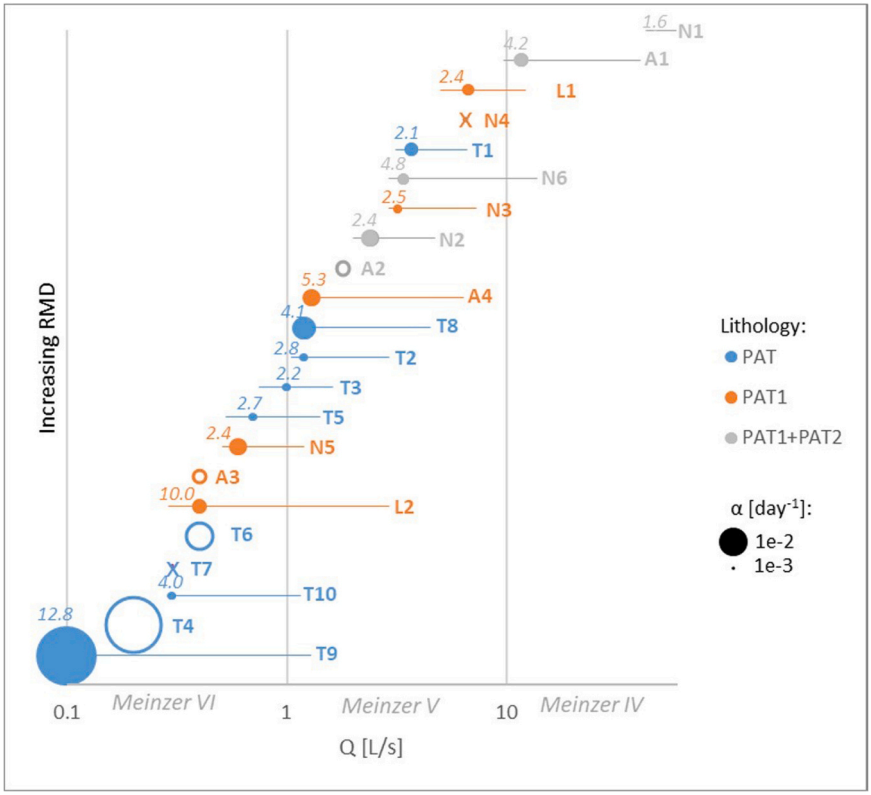

Fig. 4. Summary of the spring discharge monitoring results, considering the hydrologic year 2020–2021. Springs are ordered along the y axis based on their RMD value. The size of the circles is proportional to the coefficient of recession α. The bars indicate max and min discharge values measured along the hydrologic year. The number in italic above each circle is the spring I_v. Crosses indicate missing recession analysis and missing I_v due to a low number of discharge measurement during the low flow season. Empty circles indicate an incomplete monitoring along the hydrologic year and thus the impossibility of determining max and min annual discharge, and I_v.

variability. The distribution of I_v is fairly independent of lithology. Fourteen out of sixteen springs exhibit $I_v \leq 5.3$, indicating remarkable discharge steadiness, while I_v values from the remaining two range between 10 and 12.8.

4.4. Coefficients of effective infiltration

Hydrologic budgeting was conducted in four sectors of the study area (N, A, L, T in Fig. 2) with areal extensions ranging from 17.4 to 3.7 km^2. These sectors are plausibly "closed" in terms of groundwater flow circulation and include all the 22 springs that were monitored for discharge. Recharge was estimated between 376 mm and 292 mm across the four sectors for the hydrological year 2020–21 (Table 2), representing 36–40 % of the total precipitation, ranging from 814 to 944 mm. The total discharge from each sector varied between 163 mm and 70 mm in the same year.

From these recharge and discharge estimations, C_{EI} values were derived, ranging from 53 % to 27 %. The highest C_{EI} is associated with Sector N (53 %), which consists of PAT1+PAT2, with a predominance of PAT2 near the ground surface (see the N-N' geological cross section in Fig. 2). The second highest C_{EI} was found in Sector A (41 %), also composed of PAT1+PAT2, with PAT2 predominant in outcrop (section A-A' in Fig. 2). This is followed by Sector L, with a C_{EI} of 28 %, which is entirely composed of PAT1. The lowest C_{EI} (27 %) was identified in Sector T, which is exclusively composed of PAT.

4.5. Hydrochemistry

4.5.1. Groundwater field parameters and major ions

Considering a mean value across all measurement campaigns for each spring, the groundwater field parameters (T, EC, pH) show less variability for the springs fed by PAT compared to PAT1 and PAT1+PAT2 (Fig. 5). The PAT springs are characterized by the highest EC, with an average of 613 μS/cm, compared to 590 μS/cm in PAT1 and 587 μS/cm in PAT1+PAT2. The pH also shows slight variations among the three lithological groups, with a rising trend from PAT (7.1), to PAT1 (7.3), and PAT1+PAT2 (7.4). TDS normalized to Cl shows the lowest values in PAT1+PAT2 (35.8), suggesting that the PAT1 and PAT groups (43.7 and 47.7, respectively) have a relatively higher potential for water-rock interaction.

The major ions, sampled in two rounds, indicate that the water has a distinctly calcium-bicarbonate imprint, consistent across all springs, however some differences related to bedrock lithology can be outlined. In both sampling campaigns, PAT shows higher levels of the characteristic ions Ca and HCO_3 compared to PAT1 and PAT1+PAT2, which have similar average values, lower than PAT of approximately 25 mg/L (Ca) and 33 mg/L (HCO_3). Conversely, Mg and SO_4 are lower in PAT compared to the other two groups, with differences among the group averages of 9 mg/L and 11 mg/L, respectively. The same ratios identified for bulk rock geochemistry (Sr/Mg and Na/K) clearly differentiates springs fed by PAT showing higher ratios compared to PAT1 and PAT1+PAT2.

4.5.2. Tritium

Tritium concentration was analyzed in one spring for each of the four sectors discussed in Section 4.4. The spring with the highest RMD was chosen for each sector (i.e., N1, A1, L1, and T1), as these values likely represent larger catchment areas and therefore provide more informative data about the bulk hydrogeological features of that sector. The lowest tritium values were detected in springs L1 (1.8 TU) and N1 (1.9 TU), whereas higher values are associated with springs A1 (2.1 TU) and T1 (2.5 TU) (Fig. 6). It is worth noting that the overall variability of the tritium concentration is low, with a standard deviation of 0.3 TU. This is lower than the analytical precision associated with each measurement (0.4–0.5 TU).

Groundwater tritium concentrations from the literature for non-thermal springs arising between 400 and 900 m asl on the Adriatic side of the Northern Apennines were compared with those from this study (Fig. 6). The literature data represent typical shallow groundwater flow systems in the Northern Apennines, such as turbidite fractured aquifers (i.e. aquifer group d in Fig. 1) and associated landslides or debris deposits in the valleys of Baganza, Taro, and Secchia rivers (group f in Fig. 1) (Deiana et al., 2018, 2017; Petrella et al., 2023). Tritium data from the largest spring group in terms of discharge in the Northern Apennines (i.e., the Pojano springs) were also included. These springs fall into the III Meinzer class (RMD between 100 and 1000 L/s) and are fed by a deep karst system within Triassic evaporates pertaining to group a in Fig. 1 (Ronchetti et al., 2023). Tritium measurements in rainfall of the Northern Apennines were also considered (Deiana et al., 2018; Petrella et al., 2023). The comparison reveals that the springs sampled in this study have the lowest tritium values among those reported in the Northern Apennines literature.

Table 2
Groundwater budget of the four investigated aquifer sectors for the hydrological year 2020–2021. A: outcropping area of aquifer units; P_e: effective precipitation; TD: total discharge; C_{EI}: coefficient of effective infiltration.

ID SECTOR	A (km^2)	P_e (mm)	TD (mm)	C_{EI}
N	17.40	309	163	0.53
A	7.88	376	154	0.41
L	3.67	331	93	0.28
T	6.43	292	78	0.27

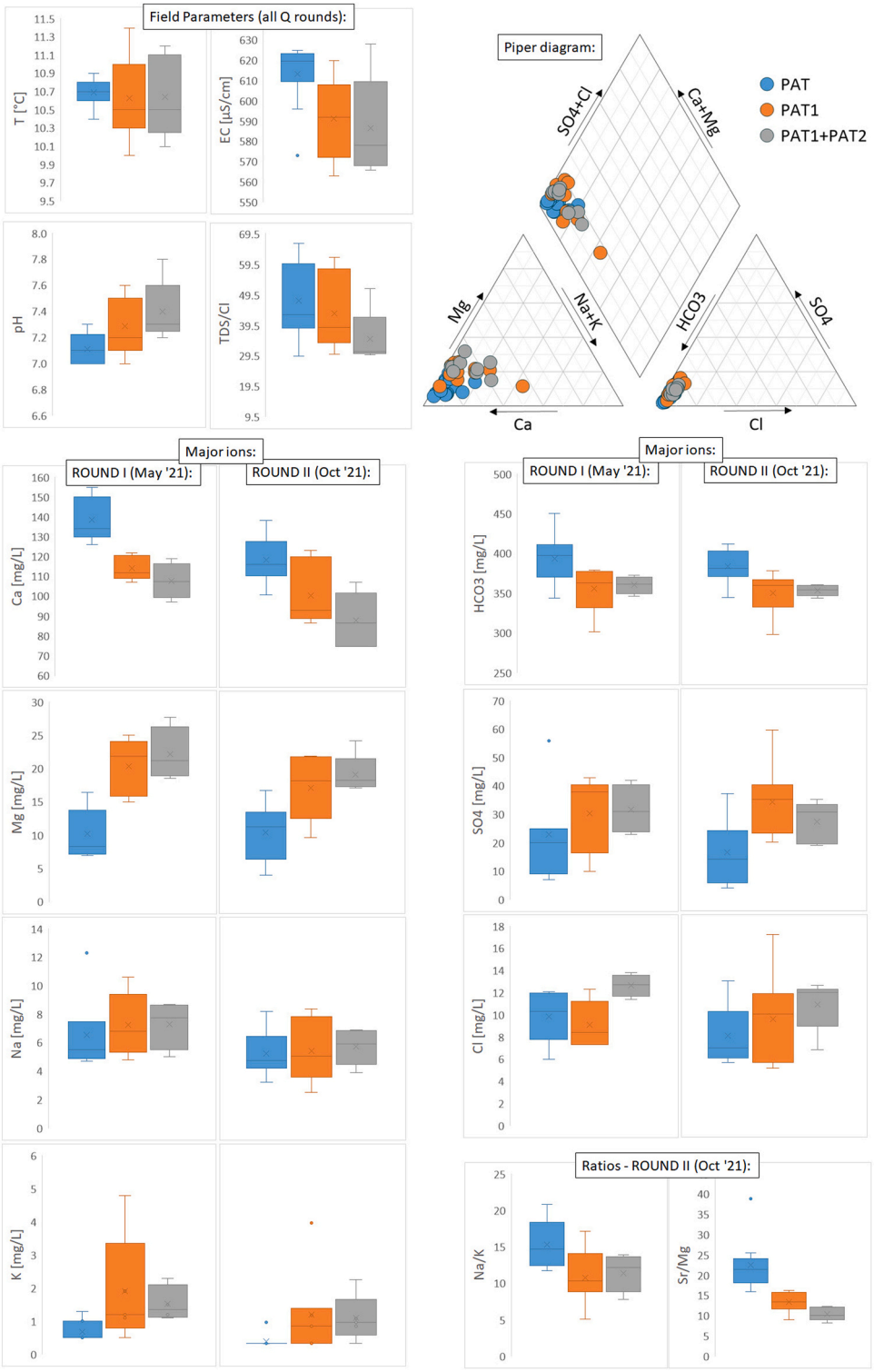

Fig. 5. spring water filed parameters (T, EC, pH, TDS/Cl) and major ions are shown as boxplots representing variability within the three lithological groups PAT1 +PAT2, PAT1, PAT. For filed parameters, the mean value of several measuring campaigns was considered for each spring. Major ions were plotted separately for the two rounds of spring water sampling. Na/K and Sr/Mg ratios were determined on molar concentrations, with Sr concentrations multiplied by 1000. On the top right angle, a Piper diagram is shown, including the results of both rounds of spring water sampling.

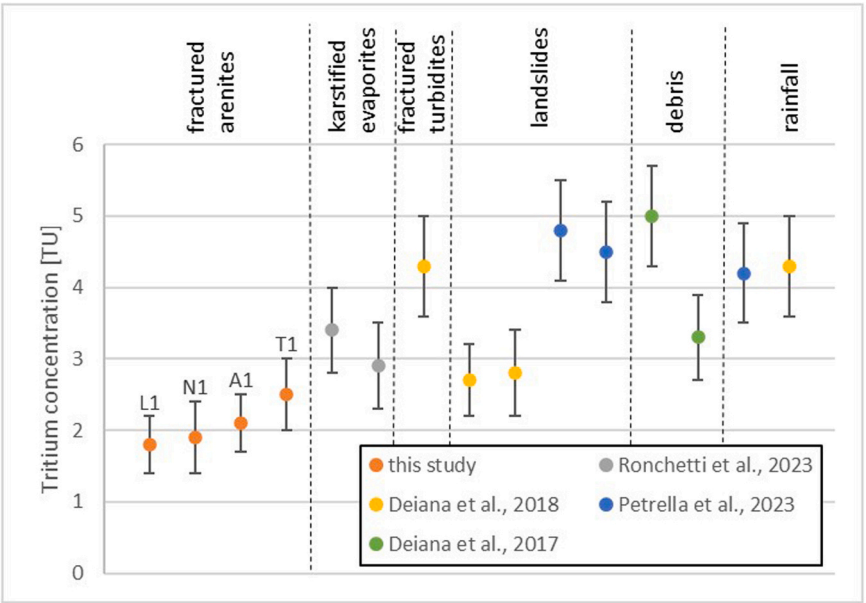

Fig. 6. Tritium concentrations (TU) in groundwater from springs fed by various lithologies in the Northern Apennines. Data include both this study and literature values. Error bars represent analytical precision.

4.6. Numerical modelling

The calibration of the two models for the hydrological year 2020–21 is considered adequate, with a NRMSE of 7.1 % and 6.2 % in the A and T sectors, respectively. The simulated hydraulic head contours of the A sector exhibits a general S-N direction, with a hydraulic gradient that progressively decreases from the upstream to the downstream regions (Fig. 7a). In the T sector, the computed

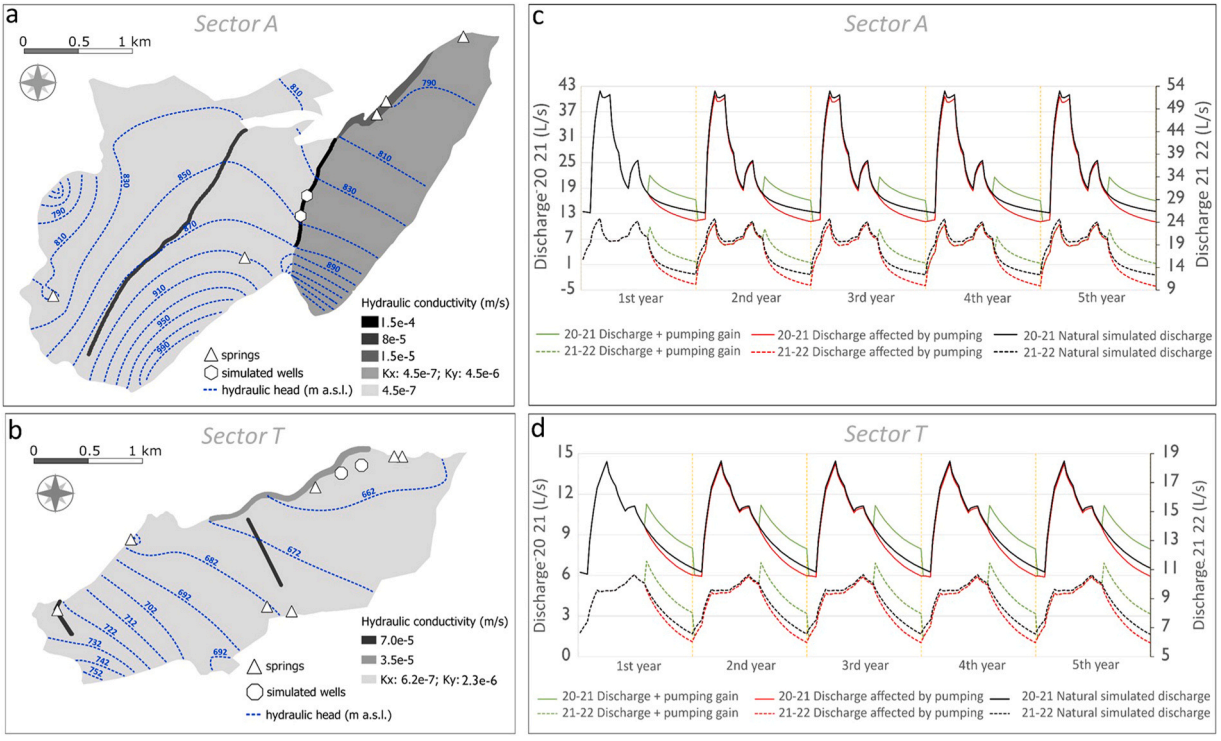

Fig. 7. Summary of modeling results: (a, b) piezometric surfaces and hydraulic conductivity distributions for sectors A and T, respectively; (c, d) simulated cumulative spring discharge under natural and pumping conditions for sectors A and T, respectively.

hydraulic heads suggest a general SW-NE flow direction, with a hydraulic gradient decreasing towards the N-NE (Fig. 7b). In both models, the flow patterns are influenced by areas of higher K which exert a draining effect.

Over the five-year simulation in natural conditions (i.e. no pumping), the mass balance of the A system yields an average annual inflow and outflow of ± 92.9 L/s considering recharge, lateral interaquifer inflows and outflows, outflows towards streams, and storage variations. The mass balance of the T sector shows an average annual inflow and outflow of ± 24.2 L/s, considering the same sinks and sources of the A sector.

In the scenarios with pumping wells, the simulations invariably suggest a gain in flow rates available for human consumption (i.e. the neat flow rate extracted from wells over the loss of natural spring and stream discharge due to pumping; Fig. 7c, d). Specifically, at the end of the five years, the gain is of 3.2 L/s and 1.5 L/s for the A and T sectors, respectively. The decrease on natural spring and stream discharges (i.e., impacts from pumping) is of −12.2 % and −2.1 % in the A sector, and −6.7 % and −16.2 % in the T sector.

The mass balances of the simulations with recharge from the hydrological year 2021–22 show an average annual inflow and outflow of ± 71.7 L/s for the A sector and of ± 18.7 L/s for the T sector. Compared to 2020–21, these results show a decrease in recharge of 26.5 % and 22.8 % for the A and T sectors, respectively, leading to a corresponding decrease in spring discharge of 17.2 % and 8.8 %. The pumping scenarios applied to the 2021–22 setup result, at the end of the fifth year, in a neat gain of 3.0 L/s and 1.4 L/s for the A and T sectors, respectively. The impact on natural discharge of springs and streams is correspondingly −14.0 % and −4.0 % in A sector and −6.8 % and −15.8 % in T sector.

5. Discussion

5.1. Sedimentary facies and their depositional environment as a proxy for aquifer performance

This section synthesizes evidence from borehole observations, pumping tests, spring discharge, water and rock chemistry, effective infiltration coefficients, and tritium analysis, collectively indicating a decline in aquifer performance with increasing distance from the paleo shoreline. The proximal members, PAT1 and PAT2, demonstrate superior performance and thus have greater potential to provide additional groundwater resources than the distal member, PAT.

-*Borehole observations* conducted in the westernmost part of the study area (A sector, Ab1 and Ab2 boreholes) reveal specific characteristics of members PAT1 and PAT2. In both cases, the groundwater flow appears to be guided by a limited number of open fractures, oriented in the Apennine and anti-Apennine directions. This is consistent with recent observations made slightly further north (N sector, Filippini et al., 2024). Notably, PAT2 is confirmed to be more heterogeneous in terms of grain size compared to PAT1 and more prone to fracturing, especially in its shallower sections, resulting in a remarkable permeability. Conversely, PAT1, which is finer-grained and lithologically homogeneous, is characterized by a very limited number of fractures with significant openings (even at considerable depths bgs). The opening and the aspect of fracture surfaces indicate the occurrence of chemical (karst) dissolution within this lithology. These open structures certainly increase the porosity and therefore the storage capacity of the rock mass. An unpublished borehole dilution test and borehole-to-spring tracer test previously conducted in the A sector using NaCl and nanoparticles showed much higher groundwater flow velocities in PAT1 and PAT2 than in all other Northern Apennine sandstone aquifers, suggesting a karst-like behavior with preferential conduits governing the groundwater flow system dynamics.

-*Pumping tests* conducted in the westernmost (A sector) and easternmost (T sector) parts of the study area indicate hydrogeological properties within the upper range of values typically found in North Apennine sedimentary fractured aquifers (Gargini et al., 2006, 2008). A decreasing gradient in bulk hydraulic conductivity is observed from west (PAT1 and PAT2, having similar properties) to east (PAT). Tests in the T sector also highlight the role of faults in increasing the hydraulic conductivity of the rock mass within their damage zone. Specifically, Tb1, located in a damage zone, shows values that are an order of magnitude higher than Tb2 in the intact rock mass.

-*Spring discharge* during the recession season (RMD) decreases from west to east across the study area, with the highest values in springs fed by PAT1 +PAT2, followed by PAT1, and the lowest values in PAT. Similarly, the coefficient of recession α increases, suggesting that the recharge basins for springs are larger in the west (PAT1 +PAT2 and PAT1) than in the east (PAT).

-*Groundwater chemistry* suggests the longest water-rock interaction time for groundwater discharging from PAT, likely associated with the lower hydraulic conductivity of the lithology. This is inferred from the greater stability of the physicochemical parameters (T, EC, pH) in PAT compared to PAT1 and PAT1 +PAT2, concurrently with the higher EC values, and higher concentrations of Ca and HCO_3. TDS normalized to Cl suggests that PAT1 +PAT2 groundwater has the lowest potential for water-rock interaction, possibly reflecting relatively quicker groundwater movement, given the close similarities in bulk rock composition of the three members. Differences in concentration of secondary ions from groundwater discharging among the three members are likely related to the chemical composition of the rock, as reflected by the similar variation of chemical indices, such as Sr/Mg and Na/K. The Sr/Mg ratio reflects slight differences in the carbonate composition, whereas Na/K suggests different degrees of involvement of plagioclase and K-feldspars in the water/rock interaction.

-*Coefficient of effective infiltration* (C_{EI}) is highest in the N and A sectors, where PAT2 predominantly crops out, and lower in the L and T sectors, characterized by PAT1 and PA exposures, respectively. This suggests that PAT2 is more prone to infiltration than all other members, most likely due to increased fragility driven by textural heterogeneity. This maximizes vertical recharge in the N and A sectors compared to L and T.

-*Tritium* levels in the main springs of the study area, despite limited variability, show the highest values in the L sector (PAT1), followed by N, A (PAT1 +PAT2), and T (PAT). This suggests that PAT1 is the member with the longest renewal times and thus the highest groundwater storage capacity (see e.g., Allen and Boutt, 2023). This would be consistent with observations from borehole Ab1,

suggesting enhanced effective porosity due to deep open fractures and karstification in PAT1. Instead, PAT2 and PAT have more limited storage capacity, probably due to their more widespread, but less open fracture systems, reasonably associated to a lower bulk porosity. The size of the recharge basin for each spring could also influence the aquifer storage capacity and consequently the variation in tritium levels. Unfortunately, the recharge basin associated with each spring cannot be defined with sufficient precision to make definitive conclusions about its sizes. However, it can be assumed that all basins are quite extensive, as they supply water to the four main springs.

In summary, sandstone aquifers formed in proximal depositional environments (members PAT1 and PAT2), both fragile and prone to karst dissolution, are characterized by an increased bulk permeability of the rock mass. A dual porosity system influences the groundwater flow within these members: a diffuse system that aids infiltration and recharge (mostly developed in PAT2, due to the higher textural heterogeneity) and a karstified system that aids overall porosity and storage (mostly developed in PAT1, due to the lower textural heterogeneity leading to a higher potential for water-rock interaction) (Fig. 8). The occurrence of preferential flowpaths in these members generates a greater hierarchy in spring arrangement (drainage towards fewer, larger springs that dry out less quickly) compared to the typical Northern Apennine setting, where a large number of diffuse low discharge outlets is generally associated with one groundwater reservoir (Gargini et al., 2008). Particularly, the combination of surficial PAT2 (high infiltration/recharge capacity) and underlying PAT1 (high storage capacity) results in the most favorable discharge settings (i.e., the only two springs in class IV within the entire study area: N1 and A1). The PAT1 aquifer alone feeds notable springs such as L1 (moderately high RMD, low alpha), as well as springs with intermediate RMD and alpha characteristics between PAT1+PAT2 and PAT. On the other hand, PAT is characterized by low infiltration and storage capacity, and a lower bulk hydraulic conductivity compared to the proximal members, resulting in lower discharge springs with a more widespread arrangement (drainage towards a greater number of smaller springs that dry out more quickly).

5.2. *Implications for groundwater management in a climate change scenario*

The low tritium levels of the main springs in the study area compared to other sites of the Northern Apennine suggest high groundwater storage capacity in the fractured arenites of the Pantano Formation. The low variability of the spring discharge (I_v) and coefficient of recession (α) compared to most of the Northern Apennine springs (Gargini et al., 2008; Segadelli et al., 2021), also indicates a good discharge capacity of the lithology. The combination of these two features demonstrates that Pantano has unique aquifer performance in the northern Apennine context, and it is therefore worth investigating further as a strategic resource in light of future climate changes.

Sandstone aquifers formed in two distinct depositional environments in terms of distance from the shoreline (proximal sector A and distal sector T), both of which have experienced recurrent supply crises in the last decades due to decreased recharge, have been modeled to test sustainable exploitation schemes through pumping in the view of future droughts. In both sectors, hydrogeological configurations have been identified that potentially host exploitable groundwater resources, the withdrawal of which would unlikely give origin to unsustainable impacts on natural discharge. The models, calibrated on a moderately dry year (2020–21) and further used

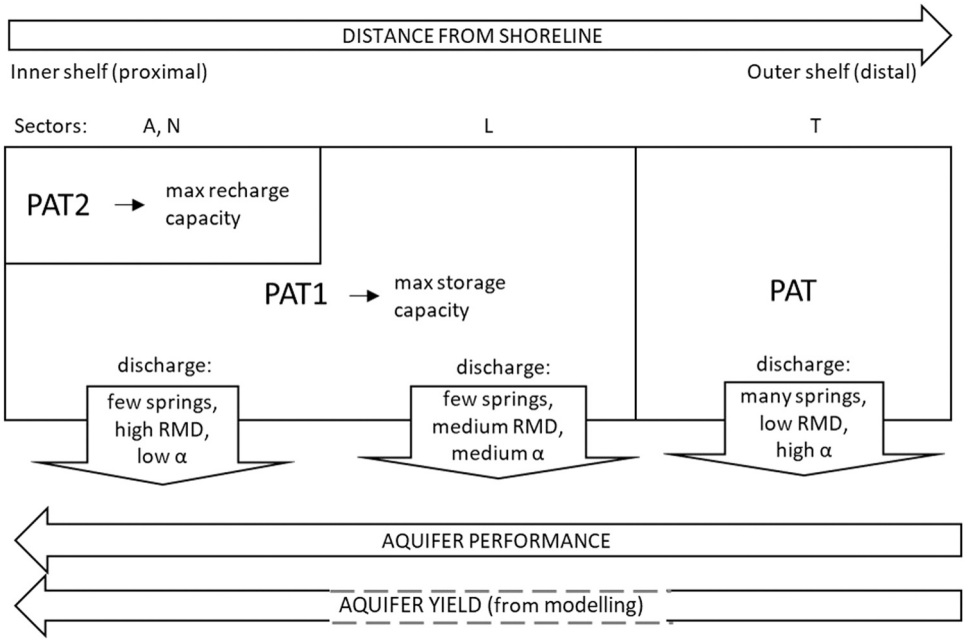

Fig. 8. Conceptual model of gradients along depositional environment, aquifer performance, and aquifer yield throughout the members of the Pantano Formation.

to simulate a severely dry year (2021–22), allowed for the definition of sustainable pumping rates (5–2 L/s, in the A and T sectors, respectively). Even in the most severe drought scenario, these rates may help overcome the known cyclic issues of drinking water supply, causing a relatively low impact on natural discharge, i.e. a decrease < 15 % of the natural spring and stream flowrate. The potential of aquifer exploitation through pumping (i.e. aquifer yield) follows the same gradient of distance from the shoreline in the depositional environment that has already been observed for aquifer performance (Fig. 8), being higher in PAT1+PAT2 (with the model suggesting a gain for human consumption through pumping of 3 L/s in 2021–22) compared to PAT (gain of 1.4 L/s in 2021–22). Therefore, the Pantano Formation is a strategic resource not only for its natural spring discharge, but also for its potential to sustainably supply groundwater through pumping, especially in areas with high storage capacity. This can help mitigate the increasing impacts of droughts on drinking water availability.

6. Conclusions

This study focused on the arenitic aquifers of the Northern Apennines, specifically examining the Miocene Pantano Formation. Through comprehensive geological, hydrological and geochemical analyses, including borehole observations, pumping tests, spring discharge measurements, groundwater chemistry assessments, coefficients of effective infiltration, and tritium analysis, it is demonstrated that aquifer performance declines as a function of the depositional environment, with increasing distance from the paleo shoreline. Proximal members (PAT1 and PAT2) show higher aquifer performance due to increased bulk permeability, a dual porosity system composed of diffuse fractures and karst conduits, facilitating infiltration and recharge, and enhancing overall porosity and storage. Conversely, the distal member (PAT) exhibits lower aptitude to infiltration, storage capacity, and hydraulic conductivity. Consequently, discharge in the proximal members is more hierarchized, with a relatively low number of highly productive springs, whereas the distal member feeds smaller and less stable springs, with a more diffuse arrangement, more prone to discharge drops induced by decreased recharge during droughts.

The Pantano Formation's unique aquifer performance, marked by high water storage capacity and stable discharge rates, positions it as a strategic groundwater resource in the Northern Apennines, especially in the context of climate change. Sustainable exploitation models suggest that, despite recent drought-induced supply crises, this aquifer can provide reliable water resources through carefully managed pumping schemes, ensuring a sustainable drinking water supply under increasingly severe drought conditions.

Mapping sedimentary facies and their related depositional environments can therefore serve as a proxy for inferring aquifer performance in other parts of the Northern Apennines where the Pantano Formation crops out, but has not yet been investigated in detail from a hydrogeological perspective. This could drive further investigation and actions to optimize the management of the resource for drinking water supply in the view of increasing droughts due to climate change.

Eventually, interpreting depositional environments as a tool for predicting aquifer performance has the potential to be further extended to other regions of the world where shallow-marine arenitic formations dominate the geological landscape.

CRediT authorship contribution statement

Maria Filippini: Writing – original draft, Visualization, Methodology, Investigation, Formal analysis, Data curation, Conceptualization. **Alessandro Amorosi:** Writing – review & editing, Writing – original draft, Methodology, Conceptualization. **Enrico Dinelli:** Writing – review & editing, Visualization, Formal analysis, Conceptualization. **Tommaso Casati:** Writing – review & editing, Writing – original draft, Visualization, Formal analysis. **Alessandro Gargini:** Writing – review & editing, Writing – original draft, Supervision, Formal analysis, Data curation, Conceptualization. **Stefano Segadelli:** Writing – review & editing, Visualization, Methodology, Investigation, Conceptualization. **Laura Landi:** Writing – review & editing, Writing – original draft, Visualization, Formal analysis.

Declaration of Competing Interest

The authors declare that they have no known competing financial interests or personal relationships that could have appeared to influence the work reported in this paper.

Acknowledgements

The authors would like to acknowledge the support of the student Daniel De Luca, whose assistance in the field was essential. They would also like to extend their gratitude to Alessandro Stefani, Andrea Bergonzoni, Stefano Venturi, and other employees of GruppoHERA, whose contributions made this investigation possible.

Appendix A. Supporting information

Supplementary data associated with this article can be found in the online version at doi:10.1016/j.ejrh.2025.102183.

Data Availability

Data will be made available on request.

References

Abdelhalim, A., Sefelnasr, A., Ismail, E., 2019. Numerical modeling technique for groundwater management in Samalut city, Minia Governorate, Egypt. Arab. J. Geosci. 12, 124.

Abusaada, M., Sauter, M., 2013. Studying the flow dynamics of a karst aquifer system with an equivalent porous medium model. Groundwater 51, 641–650.

Allen, D.J., Brewerton, L.M., Coleby, B.R., Gibbs, M.A., Lewis, A.M., MacDonald, S.J., Wagstaff, A.T., Williams, L.J., 1997. The physical properties of major aquifers in England and Wales. British Geological Survey, Nottingham, England (UK).

Allen, M., Boutt, D., 2023. Environmental Tracers Tritium 3H and SF6 used to improve knowledge of groundwater sustainability of a Crystalline Rock Island Aquifer of Tobago, West Indies. Water 15, 4231.

Amanambu, A.C., Obarein, O.A., Mossa, J., Li, L., Ayeni, S.S., Balogun, O., Oyebamiji, A., Ochege, F.U., 2020. Groundwater system and climate change: present status and future considerations. J. Hydrol. 589, 125163.

Amorosi, A., 1995. Glaucony and sequence stratigraphy; a conceptual framework of distribution in siliciclastic sequences. J. Sediment. Res. 65, 419–425.

Amorosi, A., 1997. Miocene shallow-water deposits of the northern Apennines: a stratigraphic marker across a dominantly turbidite foreland-basin succession. Geol. Mijnb. 75, 295–307.

Anderson, M.P., Woessner, W.W., Hunt, R.J., 2015. Applied Groundwater Modeling: Simulation of Flow and Advective Transport. Academic press.

Atawneh, D.A., Cartwright, N., Bertone, E., 2021. Climate change and its impact on the projected values of groundwater recharge: a review. J. Hydrol. 601, 126602.

Atekwana, E.A., Atekwana, E.A., Rowe, R.S., Werkema, D.D., Legall, F.D., 2004. The relationship of total dissolved solids measurements to bulk electrical conductivity in an aquifer contaminated with hydrocarbon. J. Appl. Geophys. 56, 281–294.

Balocchi, P., 2014. Analisi macrostrutturale e mesostrutturale del Gruppo di Bismantova affiorante tra Zocca e Castel d'Aiano (Appennino modenese e bolognese). Atti della Soc. à dei Nat. e Mat. di Modena 145, 27–42.

Bayer, P., Comunian, A., Höyng, D., Mariethoz, G., 2015. High resolution multi-facies realizations of sedimentary reservoir and aquifer analogs. Sci. Data 2, 150033.

Caloiero, T., Caloiero, P., Frustaci, F., 2018. Long-term precipitation trend analysis in Europe and in the Mediterranean basin. Water Environ. J. 32, 433–445.

Cervi, F., Petronici, F., Castellarin, A., Marcaccio, M., Bertolini, A., Borgatti, L., 2018. Climate-change potential effects on the hydrological regime of freshwater springs in the Italian Northern Apennines. Sci. Total Environ. 622-623, 337–348.

Cherry, M., Gilmore, T., Mittelstet, A., Gastmans, D., Santos, V., Gates, J.B., 2020. Recharge seasonality based on stable isotopes: nongrowing season bias altered by irrigation in Nebraska. Hydrol. Process. 34, 1575–1586.

Chiesi, M., De Waele, J., Forti, P., 2010. Origin and evolution of a salty gypsum/anhydrite karst spring: the case of Poiano (Northern Apennines, Italy). Hydrogeol. J. 18, 1111–1124.

Cuthbert, M.O., Taylor, R.G., Favreau, G., Todd, M.C., Shamsudduha, M., Villholth, K.G., MacDonald, A.M., Scanlon, B.R., Kotchoni, D.O.V., Vouillamoz, J.-M., Lawson, F.M.A., Adjomayi, P.A., Kashaigili, J., Seddon, D., Sorensen, J.P.R., Ebrahim, G.Y., Owor, M., Nyenje, P.M., Nazoumou, Y., Goni, I., Ousmane, B.I., Sibanda, T., Ascott, M.J., Macdonald, D.M.J., Agyekum, W., Koussoubé, Y., Wanke, H., Kim, H., Wada, Y., Lo, M.-H., Oki, T., Kukuric, N., 2019. Observed controls on resilience of groundwater to climate variability in sub-Saharan Africa. Nature 572, 230–234.

Deiana, M., Mussi, M., Ronchetti, F., 2017. Discharge and environmental isotope behaviours of adjacent fractured and porous aquifers. Environ. Earth Sci. 76, 595.

Deiana, M., Cervi, F., Pennisi, M., Mussi, M., Bertrand, C., Tazioli, A., Corsini, A., Ronchetti, F., 2018. Chemical and isotopic investigations (δ18O, δ2H, 3H, 87Sr/86Sr) to define groundwater processes occurring in a deep-seated landslide in flysch. Hydrogeol. J. 26, 2669–2691.

Dore, M.H.I., 2005. Climate change and changes in global precipitation patterns: what do we know? Environ. Int. 31, 1167–1181.

Filippini, M., Segadelli, S., Dinelli, E., Failoni, M., Stumpp, C., Vignaroli, G., Casati, T., Tiboni, B., Gargini, A., 2024. Hydrogeological assessment of a major spring discharging from a calcarenitic aquifer with implications on resilience to climate change. Sci. Total Environ. 913, 169770.

Folch, A., Mas-Pla, J., 2008. Hydrogeological interactions between fault zones and alluvial aquifers in regional flow systems. Hydrol. Process. 22, 3476–3487.

Gargini, A., Piccinini, L., Martelli, L., Rosselli, S., Bencini, A., Messina, A., Canuti, P., 2006. Hydrogeology of turbidites: a conceptual model derived by the geological survey of Tuscan-Emilian Apennines and the environmental monitoring for the high speed railway tunnel connection between Florence and Bologna. Boll. Soc. Geol. Ital. 125, 293–327.

Gargini, A., Vincenzi, V., Piccinini, L., Zuppi, G., Canuti, P., 2008. Groundwater flow systems in turbidites of the Northern Apennines (Italy): natural discharge and high speed railway tunnel drainage. Hydrogeol. J. 16, 1577–1599.

Gargini, A., De Nardo, M.T., Piccinini, L., Segadelli, S., Vincenzi, V., 2014. Spring discharge and groundwater flow systems in sedimentary and ophiolitic hard rock aquifers: Experiences from Northern Apennines (Italy). In: S., J.M. (Ed.), Fractured Rock Hydrogeology. CRC Press, pp. 129–143.

Gleeson, T., Wada, Y., Bierkens, M.F.P., van Beek, L.P.H., 2012. Water balance of global aquifers revealed by groundwater footprint. Nature 488, 197–200.

Goldscheider, N., Chen, Z., Auler, A.S., Bakalowicz, M., Broda, S., Drew, D., Hartmann, J., Jiang, G., Moosdorf, N., Stevanovic, Z., Veni, G., 2020. Global distribution of carbonate rocks and karst water resources. Hydrogeol. J. 28, 1661–1677.

Gossel, W., Ebraheem, A.M., Wycisk, P., 2004. A very large scale GIS-based groundwater flow model for the Nubian sandstone aquifer in Eastern Sahara (Egypt, northern Sudan and eastern Libya). Hydrogeol. J. 12, 698–713.

Green, T.R., Taniguchi, M., Kooi, H., Gurdak, J.J., Allen, D.M., Hiscock, K.M., Treidel, H., Aureli, A., 2011. Beneath the surface of global change: Impacts of climate change on groundwater. J. Hydrol. 405, 532–560.

Heiri, O., Lotter, A.F., Lemcke, G., 2001. Loss on ignition as a method for estimating organic and carbonate content in sediments: reproducibility and comparability of results. J. Paleolimnol. 25, 101–110.

Herschy, R., 1993. The velocity-area method. Flow. Meas. Instrum. 4, 7–10.

Hubert, E., Wolkersdorfer, C., 2015. Establishing a conversion factor between electrical conductivity and total dissolved solids in South African mine waters. Water S. A 41, 490–500.

Kresic, N., Stevanovic, Z., 2010. Groundwater Hydrology of Springs: Engineering, Theory, Management, and Sustainability. Butterworth-Heinemann, Oxford, UK.

Kruseman, G., Ridder, N., 1990. Analysis and evaluation of pumping test data.

Kundzewicz, Z.W., Doli, P., 2009. Will groundwater ease freshwater stress under climate change? Hydrol. Sci. J. 54, 665–675.

Lachassagne, P., Wyns, R., Dewandel, B., 2011. The fracture permeability of Hard Rock Aquifers is due neither to tectonics, nor to unloading, but to weathering processes. Terra Nova 23, 145–161.

Lorenzi, V., Banzato, F., Barberio, M.D., Goeppert, N., Goldscheider, N., Gori, F., Lacchini, A., Manetta, M., Medici, G., Rusi, S., Petitta, M., 2024. Tracking flowpaths in a complex karst system through tracer test and hydrogeochemical monitoring: implications for groundwater protection (Gran Sasso, Italy). Heliyon 10, e24663.

Maillet, E.T., 1905. Essais d'hydraulique souterraine & fluviale. A. Hermann, Paris.

Maliva, R.G., 2016. Fractured Sedimentary Rock Aquifers, Aquifer Characterization Techniques. Springer Hydrogeology.

Manga, M., 1997. A model for discharge in spring-dominated streams and implications for the transmissivity and recharge of quaternary volcanics in the Oregon Cascades. Water Resour. Res. 33, 1813–1822.

Margat, J., Van der Gun, J., 2013. Groundwater Around the World. A Geographic Synopsis. CRC press Taylor & Francis group, Boca Raton (FL, USA).

Martínez-Santos, P., Díaz-Alcaide, S., Castaño-Castaño, S., Hernández-Espriú, A., 2014. Modelling discharge through artesian springs based on a high-resolution piezometric network. Hydrol. Process. 28, 2251–2261.

Maurice, L.D., Atkinson, T.C., Barker, J.A., Williams, A.T., Gallagher, A.J., 2012. The nature and distribution of flowing features in a weakly karstified porous limestone aquifer. J. Hydrol. 438-439, 3–15.

Medici, G., West, L.J., Mountney, N.P., 2016. Characterizing flow pathways in a sandstone aquifer: tectonic vs sedimentary heterogeneities. J. Contam. Hydrol. 194, 36–58.
Medici, G., West, L.J., Mountney, N.P., Welch, M., 2019. Permeability of rock discontinuities and faults in the Triassic Sherwood Sandstone Group (UK): insights for management of fluvio-aeolian aquifers worldwide. Hydrogeol. J. 27, 2835–2855.
Medici, G., Smeraglia, L., Torabi, A., Botter, C., 2021. Review of modeling approaches to groundwater flow in deformed carbonate aquifers. Groundwater 59, 334–351.
Medici, G., Lorenzi, V., Sbarbati, C., Manetta, M., Petitta, M., 2023. Structural classification, discharge statistics, and recession analysis from the springs of the Gran Sasso (Italy) carbonate aquifer; comparison with selected analogues worldwide. Sustainability 15, 10125.
Medici, G., Munn, J.D., Parker, B.L., 2024. Delineating aquitard characteristics within a Silurian dolostone aquifer using high-density hydraulic head and fracture datasets. Hydrogeol. J. 32, 1663–1691.
Meinzer, O.E., 1923. Outline of ground-water hydrology, with definitions. Water Supply Paper 494. United States Geological Survey, Washington, D.C., pp. 1–69
Michael, H.A., Voss, C.I., 2009. Controls on groundwater flow in the Bengal Basin of India and Bangladesh: regional modeling analysis. Hydrogeol. J. 17, 1561–1577.
Miller, W.R., 1999. Geochemical baselines and maps showing acid-neutralizing capacity and potential release of total dissolved solids of stream and spring waters from different rock compositional types from mountainous watersheds in the Gunnison, Uncompahgre, and Grand Mesa National Forest, Colorado, Open-File Report, - ed.
Miller, W.R., 2002. Influence of rock composition on the geochemistry of stream and spring waters from mountainous watersheds in the Gunnison, Uncompahgre, and Grand Mesa National Forests, Colorado, Professional Paper, Version 1.0 ed.
Molz, F.J., Boman, G.K., Young, S.C., Waldrop, W.R., 1994. Borehole flowmeters: field application and data analysis. J. Hydrol. 163, 347–371.
Nastev, M., Rivera, A., Lefebvre, R., Martel, R., Savard, M., 2005. Numerical simulation of groundwater flow in regional rock aquifers, southwestern Quebec, Canada. Hydrogeol. J. 13, 835–848.
Neuman, S.P., 2005. Trends, prospects and challenges in quantifying flow and transport through fractured rocks. Hydrogeol. J. 13, 124–147.
Panini, F., Bettelli, G., Pizziolo, M., DI, C.C., Amorosi, A., Basoli, R., Bonazzi, U., Borsetti, A., Capitani, M., Fioroni, C., 2003. Carta Geologica Regionale alla scala 1: 25.000 della Regione Emilia-Romagna," Vergato"-237 SO. Foglio 237" Sasso Marconi" (Geological Map of the Emilia Romagna Region 1:25.000, "Vergato" -237 SO. Sheet 237 "Sasso Marconi"). S. EL. CA Firenze.
Peña-Angulo, D., Vicente-Serrano, S.M., Domínguez-Castro, F., Lorenzo-Lacruz, J., Murphy, C., Hannaford, J., Allan, R.P., Tramblay, Y., Reig-Gracia, F., El Kenawy, A., 2022. The complex and spatially diverse patterns of hydrological droughts across Europe. Water Resour. Res. 58, e2022WR031976.
Petrella, E., Raimondo, M., Chelli, A., Valentino, R., Severini, E., Diena, M., Celico, F., 2023. Processes and factors controlling the groundwater flow in a complex landslide: a case study in the northern Italy. Hydrol. Process. 37, e14891.
Pierce, S.A., Sharp, J.M., Guillaume, J.H.A., Mace, R.E., Eaton, D.J., 2013. Aquifer-yield continuum as a guide and typology for science-based groundwater management. Hydrogeol. J. 21, 331–340.
Powell, O., Fensham, R., 2016. The history and fate of the Nubian Sandstone Aquifer springs in the oasis depressions of the Western Desert, Egypt. Hydrogeol. J. 24, 395–406.
Rakovec, O., Samaniego, L., Hari, V., Markonis, Y., Moravec, V., Thober, S., Hanel, M., Kumar, R., 2022. The 2018–2020 multi-year drought sets a new benchmark in Europe. Earth's. Future 10, e2021EF002394.
Renken, R.A., 1996. Hydrogeology of the Southeastern Coastal Plain aquifer system in Mississippi, Alabama, Georgia, and South Carolina, Professional Paper, - ed.
Ricci Lucchi, F., 1986. The oligocene to recent foreland basins of the Northern Apennines. Foreland Basins 103–139.
Riedel, T., Weber, T.K.D., 2020. Review: The influence of global change on Europe's water cycle and groundwater recharge. Hydrogeol. J. 28, 1939–1959.
Ronchetti, F., Deiana, M., Lugli, S., Sabattini, M., Critelli, V., Aguzzoli, A., Mussi, M., 2023. Water isotope analyses and flow measurements for understanding the stream and meteoric recharge contributions to the Poiano evaporite karst spring in the North Apennines, Italy. Hydrogeol. J. 31, 601–619.
Runkel, A.C., Tipping, R.G., Alexander, E.C., Alexander, S.C., 2006. Hydrostratigraphic characterization of intergranular and secondary porosity in part of the Cambrian sandstone aquifer system of the cratonic interior of North America: Improving predictability of hydrogeologic properties. Sediment. Geol. 184, 281–304.
Saar, M.O., Manga, M., 2004. Depth dependence of permeability in the Oregon Cascades inferred from hydrogeologic, thermal, seismic, and magmatic modeling constraints. J. Geophys. Res.: Solid Earth 109.
Scanlon, B.R., Mace, R.E., Barrett, M.E., Smith, B., 2003. Can we simulate regional groundwater flow in a karst system using equivalent porous media models? Case study, Barton Springs Edwards aquifer, USA. J. Hydrol. 276, 137–158.
Scanlon, B.R., Fakhreddine, S., Rateb, A., de Graaf, I., Famiglietti, J., Gleeson, T., Grafton, R.Q., Jobbagy, E., Kebede, S., Kolusu, S.R., Konikow, L.F., Long, D., Mekonnen, M., Schmied, H.M., Mukherjee, A., MacDonald, A., Reedy, R.C., Shamsudduha, M., Simmons, C.T., Sun, A., Taylor, R.G., Villholth, K.G., Vörösmarty, C.J., Zheng, C., 2023. Global water resources and the role of groundwater in a resilient water future. Nat. Rev. Earth Environ. 4, 87–101.
Schäfer, I., Hebert, D., Zeiske, U., 2000. On low-level tritium measurements with LSC Quantulus. Appl. Radiat. Isot. 53, 309–315.
Segadelli, S., Vescovi, P., Chelli, A., Petrella, E., De Nardo, M.T., Gargini, A., Celico, F., 2017a. Hydrogeological mapping of heterogeneous and multi-layered ophiolitic aquifers (Mountain Prinzera, northern Apennines, Italy). J. Maps 13, 737–746.
Segadelli, S., Vescovi, P., Ogata, K., Chelli, A., Zanini, A., Boschetti, T., Petrella, E., Toscani, L., Gargini, A., Celico, F., 2017b. A conceptual hydrogeological model of ophiolitic aquifers (serpentinised peridotite): the test example of Mt. Prinzera (Northern Italy). Hydrol. Process. 31, 1058–1073.
Segadelli, S., Filippini, M., Monti, A., Celico, F., Gargini, A., 2021. Estimation of recharge in mountain hard-rock aquifers based on discrete spring discharge monitoring during base-flow recession. Hydrogeol. J. 29, 949–961.
Shakeel, A., Ramaswamy, J., Abdin, S., 2008. Groundwater Dynamics in Hard Rock Aquifers. Springer, New York.
Singhal, B.B.S., Gupta, R.P., 2010. Applied Hydrogeology of Fractured Rocks.
Sophocleous, M.A., Koelliker, J.K., Govindaraju, R.S., Birdie, T., Ramireddygari, S.R., Perkins, S.P., 1999. Integrated numerical modeling for basin-wide water management: the case of the Rattlesnake Creek basin in south-central Kansas. J. Hydrol. 214, 179–196.
Steenhuis, T.S., Van Der Molen, W.H., 1986. The Thornthwaite-Mather procedure as a simple engineering method to predict recharge. J. Hydrol. 84, 221–229.
Stevanović, Z., 2019. Karst waters in potable water supply: a global scale overview. Environ. Earth Sci. 78, 662.
Stigter, T.Y., Miller, J., Chen, J., Re, V., 2023. Groundwater and climate change: threats and opportunities. Hydrogeol. J. 31, 7–10.
Tambe, S., Kharel, G., Arrawatia, M.L., Kulkarni, H., Mahamuni, K., Ganeriwala, A.K., 2012. Reviving dying springs: climate change adaptation experiments from the Sikkim Himalaya. Mt. Res. Dev. 32, 62–72, 11.
Taylor, R.G., Scanlon, B., Döll, P., Rodell, M., van Beek, R., Wada, Y., Longuevergne, L., Leblanc, M., Famiglietti, J.S., Edmunds, M., Konikow, L., Green, T.R., Chen, J., Taniguchi, M., Bierkens, M.F.P., MacDonald, A., Fan, Y., Maxwell, R.M., Yechieli, Y., Gurdak, J.J., Allen, D.M., Shamsudduha, M., Hiscock, K., Yeh, P.J.F., Holman, I., Treidel, H., 2013. Ground water and climate change. Nat. Clim. Change 3, 322–329.
Thornthwaite, C., Mather, J., 1957. Instructions and tables for computing potential evapotranspiration and the water balance, publications in climatology 10/3. Centerton: Drexel Institute of Technology.
van Tonder, G.J., Botha, J.F., Chiang, W.H., Kunstmann, H., Xu, Y., 2001. Estimation of the sustainable yields of boreholes in fractured rock formations. J. Hydrol. 241, 70–90.
Trenberth, K.E., Jones, P.D., Ambenje, P., Bojariu, R., Easterling, D., Klein Tank, A., Parker, D., Rahimzadeh, F., Renwick, J.A., Rusticucci, M., 2007. Observations. surface and atmospheric climate change. Chapter 3.
Tügel, F., Houben, G., Graf, T., 2016. How appropriate is the Thiem equation for describing groundwater flow to actual wells? Hydrogeol. J. 24.
Van der Gun, J., 2022. Large Aquifer Systems Around the World. The Groundwater Project, Guelph, Ontario, Canada.
Weissinger, R., Philippi, T.E., Thoma, D., 2016. Linking climate to changing discharge at springs in Arches National Park, Utah, USA. Ecosphere 7, e01491.
WWAP, 2015. The United Nations World Water Development Report 2015: Water for a Sustainable World. Unesco, Paris.
Zhou, H., Gómez-Hernández, J.J., Li, L., 2014. Inverse methods in hydrogeology: evolution and recent trends. Adv. Water Resour. 63, 22–37.